

Numerical Analysis of Collective Neutrino Oscillations in Dense Neutrino Media

Eric Putney

12 May, 2020

Contents

Abstract	3
1 Introduction	4
1.1 Neutrinos	4
1.1.1 Flavor oscillations	4
1.1.2 Neutrino-lepton couplings	5
1.2 Core-collapse supernovae	6
2 Studying Dense Neutrino Gases	6
2.1 The density matrix and polarization vector	7
2.2 The two-angle 2D line model	9
2.3 Unitarity of the polarization vector	11
2.4 Unitarity violation	12
3 Addressing Fine Structure	13
3.1 Element-wise interpolation of the polarization vector	14
3.2 Angular dispersion on the unit sphere	14
3.3 Fine structure smoothing — spherical interpolation	17
3.3.1 Geodesics	18
3.3.2 Quaternion interpolation and Squad	19
3.4 Outlook for fine structure smoothing	22
3.5 The multi-angle 2D line model	23
4 Conclusions	25
Acknowledgements	25
Appendices	26
A Trajectory computation using Squad	26
B Animate angular dispersion, color by unitarity violation	27
Bibliography	31

Abstract

Core collapse supernovae (CCSNe) are some of the most energetic events we observe in the universe. Despite being incredibly bright electromagnetically, it is believed that nearly all of the energy released by these exploding stars is in the form of neutrinos. Due to this energetic dominance, neutrinos have become central to the study of CCSN dynamics. Neutrinos are responsible for reviving the stalled shock wave of out-flowing stellar material, triggering a dramatic explosion. Neutrinos likely also influence nucleosynthesis processes in supernovae, as their behaviors will influence the relative number densities of neutrons and protons. It has also been proposed that collective flavor oscillation of dense neutrino gases could further influence CCSN development. Investigating models that leverage simplified geometries provides unique insight into the core dynamics of these dense neutrino gases without moving to excessively complex, fully three-dimensional simulations. Previous analysis of the two-angle line model have suggested that the flavor composition of the neutrino gas at large radii saturates to a constant value. In addition, this saturation behavior is insensitive to the form of initial flavor perturbation supplied. Unfortunately, the two-angle line model is plagued by the development of fine structure that cannot be sampled by the spatial resolution of our simulation. This effect limits the distance scales accessible to the two-angle line model. We investigate novel geometric methods for eliminating small regions of very small scale structure that would allow simulations of the two-angle line model to extend farther into the non-linear regime of the neutrino gas. Additionally we explore the multi-angle line model, a revision of the two-angle line model, as a candidate for the next generation of dense neutrino gas simulations. By continuing to develop and examine increasingly physically representative models, we can be guided by our understanding of simpler models. We find that the multi-angle line model seems to resolve the issue of fine structure that limited the two-angle line model, however it remains to be confirmed whether or not flavor saturation still occurs. When a holistic understanding of neutrino flavor dynamics in the extreme environment of a CCSN is built from the study of all of these models, the extent of the role collective neutrino oscillations play in CCSNe will be made clear.

1 Introduction

1.1 Neutrinos

Neutrinos are ghostly, near-massless particles that stream through Earth’s atmosphere and all around us in staggering quantities. Neutrinos do not interact with normal matter very often, so we do not usually notice them despite their overwhelming presence. They are electrically neutral Fermions, which do not interact electromagnetically. Neutrinos are also colorless, so they do not interact via the nuclear strong force that binds nuclei together. Instead, they only interact via the weak nuclear force and the gravitational force (the latter is extremely weak due to their tiny masses).

Most of the neutrinos around us were produced in staggering quantities by the nuclear processes of the sun. Those that reach us traveled towards the earth, streaking through the atmosphere, through cities, mountains, and people into the ground. They travel through the planet’s core and then out the other side of the Earth. Because there are so many neutrinos incident on the Earth, some do occasionally knock into other particles. On average, a person has a 25% chance to be struck by a neutrino sometime in their life.

If neutrinos are so elusive, how do we know that they exist? The first indirect evidence of neutrinos came from the continuous energy spectrum of electrons emitted by beta decay. Originally it was believed that beta decay, the change of a neutron to a proton inside a nucleus, resulted in two final particles. In such a case, the energies of the final particles would be uniquely determined by conservation of energy and momentum. Experiments revealed that these energies could actually take on a continuous spectrum of values. In 1934, Enrico Fermi suggested that an unknown third particle (a neutrino) must have been emitted that experiments could not detect [1].

Direct detection of neutrinos requires some patience. When neutrinos interact with the electrons in an atom, high energy electrons are created that generate Cherenkov radiation. This radiation can then be detected by instrumentation sensitive to single photons. By closely monitoring a large region of dense matter, it is likely a neutrino will interact with an atom and generate this signal. Neutrinos were first directly detected by Cowan and Reines in 1956 [2] by placing large water tanks near a nuclear reactor and watching for Cherenkov light using extremely sensitive photomultiplier tubes.

There are three types of neutrinos, differentiated by their lepton *flavors*. These three neutrino flavors reflect the flavors of the charged leptons, i.e. the electron, muon and tau, and are named accordingly: the electron neutrino, the muon neutrino, and the tau neutrino. What are the masses of these three neutrinos? It turns out that this is not such a straightforward question to ask, and that we need to reformulate this question with some basic quantum mechanics.

1.1.1 Flavor oscillations

The Standard Model of particle physics predicts that all neutrinos are completely massless. We now know that neutrinos have non-zero masses due to the discovery of neutrino oscillations, the seemingly inexplicable transmutation of neutrinos from one type to another. Neutrino masses are the result of physics beyond the Standard Model, and the explanation for why they have mass is still unknown. Additionally, the masses of the neutrinos and their relative ordering or hierarchy is an open question in particle physics. The latter is often referred to as the neutrino mass hierarchy problem.

When neutrinos are produced in weak interactions, they are produced in a definite flavor state. In the sun, neutrinos are almost always produced in the electron flavor state. However, only the mass states of the neutrino are eigenstates of the neutrino’s vacuum Hamiltonian H_{vac} . While a

neutrino is produced in one flavor state, the process that dictates its behavior in free space depends on its combination of multiple mass states. Therefore each flavor state must be expressed as a linear combination of three mass states.

In the simplified case where there are only two neutrino flavors and masses, this relationship is given as

$$|\nu_e\rangle = \cos\theta|m_1\rangle + \sin\theta|m_2\rangle \quad \text{and} \quad |\nu_\mu\rangle = -\sin\theta|m_1\rangle + \cos\theta|m_2\rangle \quad (1)$$

where θ is the parameter that controls the mixing of flavor and mass states, known as the mixing angle. The three flavor case is qualitatively similar but is more mathematically cumbersome to present. In this form, it is clear that the transformation from the mass basis to the flavor basis is achieved by a straightforward unitary transformation.

This is the mechanism responsible for neutrino oscillations. As the neutrino propagates, the phase of each mass state evolves differently, so that the linear combination of mass states changes. When one measures the flavor state of that neutrino after it travels for some time, they could find an electron neutrino or something else, such as a muon or tau neutrino.

1.1.2 Neutrino-lepton couplings

Neutrino oscillations vary drastically when one leaves the vacuum for regions with high number densities of other leptons. These neutrino-lepton scattering processes are represented schematically in Fig. 1. In dense regions of matter such as the sun, coherent forward scattering of neutrinos off electrons adjusts their oscillation dynamics (see Fig. 1). When neutrinos pass through regions with a large matter density, flavor dynamics are affected in an analogous way to how light acquires an index of refraction when it passes through matter. An example of this is the Mikheyev–Smirnov–Wolfenstein (MSW) effect induces resonant flavor conversion of neutrinos (see Fig. 1). For a more detailed review, see Ref. [3]. Understanding the MSW effect eventually resolved the famous solar neutrino problem, where fewer electron neutrinos were detected from the sun than expected. The Homestake experiment in the 1960s was the first to observe this deficit [4].

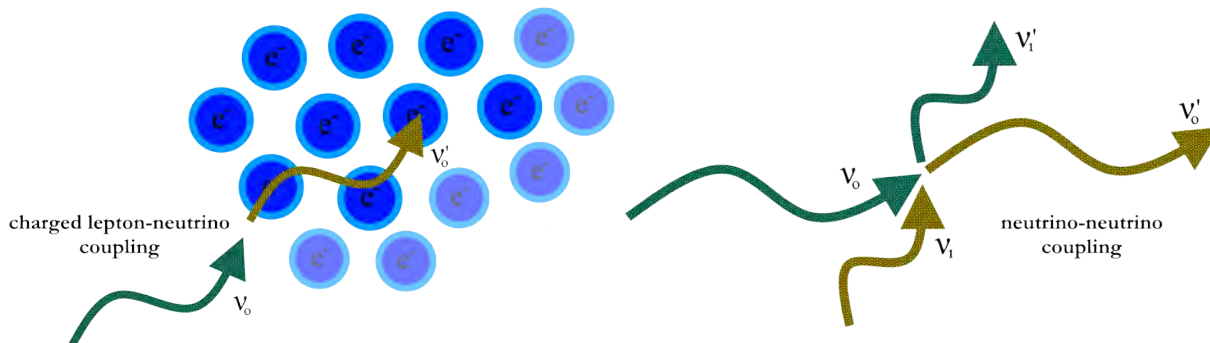


Figure 1: A cartoon depiction of neutrino-lepton scattering processes, neutrino momentum is indicated by the wavelength whereas neutrino flavor is indicated by the color. Coherent forward scattering off nearby leptons adjusts neutrino flavor oscillation.

Neutrinos also couple and scatter off of other nearby neutrinos. This process depends on the number density of neutrinos n_ν , and is typically very small. The potential generated by neutrino-neutrino scattering is only significant within regions with very large neutrino number densities such as inside core-collapse supernovae (CCSNe). In addition, the scattering potential depends on the incident angle between two neutrinos, bringing the geometry of the interaction to the forefront.

Section 2.1 introduces this potential explicitly. Further details regarding the neutrino-neutrino scattering potential may be found in Refs. [5] and [6]. It is important to note that the self-coupling of the neutrino gas from this neutrino-neutrino scattering is a non-linear effect. This non-linearity makes studying dense neutrino gases a challenging task both analytically and numerically.

1.2 Core-collapse supernovae

The primary motivation for studying the development of these dense neutrino gases is to understand their role in extreme astronomical environments. Neutrinos are produced in staggering quantities by CCSNe and neutron star mergers. It is estimated that nearly 99% of the energy released in a CCSN is carried away by neutrinos. In the first ten seconds of the explosion, up to 10^{58} neutrinos can be emitted. Understanding this, it is natural to ask if neutrinos and neutrino oscillations have an effect on CCSNe. The complex dynamics of neutrino oscillations in CCSNe are not well understood, although Refs. [7–11] have argued that collective neutrino oscillations could hold a number of significant implications for CCSNe. However, it has been well established that neutrinos themselves are essential to CCSNe for reasons we will now discuss.

Neutrinos are dominant in the energetic processes of supernovae. It is believed that this burst of neutrinos is responsible for reviving the shock of the supernova, and is therefore the main driver of the explosion [12]. While the trillions of neutrinos that pass through our bodies may never interact with us, the astronomical density of neutrinos in supernovae makes it very likely that this gas of neutrinos will interact with matter in a significant way. When this happens, the neutrino can either scatter off the target or be absorbed. Scattering events do not efficiently transfer energy from neutrinos to matter, however the absorption of a neutrino by a neutron in stimulated beta decay transfers energy very efficiently. Stimulated beta decay is the capture of an electron neutrino by a neutron. It is typically written as follows

$$\nu_e + n \longrightarrow p + e^- \quad (2a)$$

Whereas inverse stimulated beta decay, the capture of an electron antineutrino by a proton, goes as

$$\bar{\nu}_e + p \longrightarrow n + e^+ \quad (2b)$$

The rate at which these processes occur is sensitive to the number densities of protons/neutrons as well as electron neutrinos/antineutrinos. It is clear that neutrinos (and possibly their flavor dynamics as well) play an important role in determining the ratio of neutrons to protons in the supernova medium. This ratio fundamentally constrains what elements can be produced through supernova nucleosynthesis. The impacts of neutrino capture on the CCSN r-processes (a set of nuclear processes where heavy nuclei are created via rapid neutron capture) are discussed in Ref. [13], whereas the potential role collective neutrino oscillations might play in CCSN r-processes is examined in Ref. [14]. The growing consensus is that we need an accurate picture of the flavor content of the neutrino gas to understand how it will interact with the surrounding supernova medium. Studying the behaviors of these dense neutrino gases will better our understanding of supernova explosion dynamics, nucleosynthesis, as well as the expected neutrino signal when we observe neutrinos from future supernovae.

2 Studying Dense Neutrino Gases

Dense neutrino gases are an important consideration in the study of core-collapse supernovae. This section begins by introducing the mathematical language used when approaching this problem, and

then introduces the two-angle neutrino line model. A brief review of other analyses of the two-angle line model is provided, followed by a discussion the two-angle line model’s biggest constraint: violation of unitarity.

2.1 The density matrix and polarization vector

This problem is more handily solved using alternative mathematical formalisms of quantum mechanics versus the traditional wavefunction formalism. First, it is convenient to discuss the density matrix. The quantum-mechanical density matrix provides a statistical description of states in a system, and can describe both pure and mixed states. We will apply the two-flavor approximation in this analysis. In this approximation, the neutrino flavor ν_τ is a linear combination of both ν_μ, ν_τ flavor states. In the two-flavor case, the density matrix is expressed in the flavor basis as

$$\rho = \begin{bmatrix} \rho_{ee} & \rho_{e\tau} \\ \rho_{\tau e} & \rho_{\tau\tau} \end{bmatrix}. \quad (3)$$

When appropriately normalized, the diagonal elements of the density matrix are interpreted as statistical measurement probabilities. ρ_{ee} is the probability of measuring the system in the electron neutrino state, while $\rho_{\tau\tau}$ is the probability of measuring the system in the tau neutrino state. Note that for this choice of normalization $0 \leq \rho_{ee}, \rho_{\tau\tau} \leq 1$ and $\rho_{ee} + \rho_{\tau\tau} = 1$. Both quantities are real. The off-diagonal element $\rho_{e\tau}$ and its conjugate represent the quantum-mechanical coherence between the electron and tau flavor states. The most abundant neutrino species in supernovae are electron neutrinos. Throughout this work, we initialize the state of the neutrino gas in the electron neutrino state with a small perturbation ϵ to its coherence. This corresponds to the density matrix $\rho = \begin{bmatrix} 1 & \epsilon \\ \epsilon^* & 0 \end{bmatrix}$. Because the neutrinos begin in the electron neutrino state, ρ_{ee} is referred to as the “survival probability” of the electron neutrino whereas $\rho_{\tau\tau}$ is the probability it has oscillated out of the electron neutrino state.

This density matrix is Hermitian, so the two off-diagonal elements are conjugates of one another. With this in mind, we can rewrite the density matrix as

$$\rho = \begin{bmatrix} \rho_{ee} & \rho_{e\tau} \\ \rho_{e\tau}^* & \rho_{\tau\tau} \end{bmatrix}. \quad (4)$$

The trace of the density matrix is just the summed probability of every measurable state, therefore

$$\text{Tr}(\rho) = \rho_{ee} + \rho_{\tau\tau} = 1. \quad (5)$$

The flavor content of the gas is represented by a quantum mechanical pure state. Therefore the density matrix is idempotent i.e. $\rho^2 = \rho$. Note that this also implies that the trace of the square of the density matrix must be equal to one

$$\text{Tr}(\rho^2) = 1. \quad (6)$$

The general equation of motion in the density matrix formalism is given by the von Neumann equation

$$i\hbar \frac{d}{dt} \rho(t) = [\text{H}, \rho(t)]. \quad (7)$$

The particular Hamiltonian H used that accounts for the various potentials encountered in dense neutrino gas will be discussed at the end of this section. There is another way to represent these three parameters ($\rho_{ee}, \text{Re}(\rho_{e\tau}), \text{Im}(\rho_{e\tau})$) that holds an interesting geometric interpretation. Note

that these three parameters are not all independent, and that two of these parameters are necessarily constrained by Eq. (5). Much like points on the surface of a 3-dimensional unit sphere, these three coordinates only represent two free parameters. We will map these density matrix elements onto a vector that spans the surface of a unit sphere, i.e. a sphere of radius 1. This is the polarization vector \vec{P} formalism.

This mapping can be extracted in a straightforward manner by breaking down the 2×2 Hermitian matrix ρ into a linear combination of orthogonal (via the Hilbert-Schmidt inner product) basis elements. This set is I_2 and the Pauli matrices $\sigma_1 = \begin{bmatrix} 0 & 1 \\ 1 & 0 \end{bmatrix}$, $\sigma_2 = \begin{bmatrix} 0 & -i \\ i & 0 \end{bmatrix}$, $\sigma_3 = \begin{bmatrix} 1 & 0 \\ 0 & -1 \end{bmatrix}$. This linear combination is written as follows

$$\rho = \frac{1}{2}(\text{Tr}(\rho)I_2 + \vec{P} \cdot \vec{\sigma}) \quad (8)$$

where $\vec{\sigma}$ is the vectorized representation of the Pauli matrices, and $\text{Tr}(\rho) = 1$ as before. The leading factor of $1/2$ comes from normalizing these orthogonal Pauli matrices by the Hilbert-Schmidt norm of each Pauli matrix to produce an orthonormal basis. Here, the components of the polarization vector \vec{P} represent the components of the linear combination of the Pauli matrices that compose ρ . A quick method to extract these components is to compute the Hilbert-Schmidt inner product of ρ and the Pauli matrices. The Hilbert-Schmidt inner product of two matrices A and B is defined as the trace of the product of A^* and B

$$\langle A, B \rangle_{\text{HS}} = \text{Tr}(A^*B). \quad (9)$$

Computing this inner product for all three Pauli matrices, we find that \vec{P} is expressed as follows

$$\vec{P} = \begin{bmatrix} 2\text{Re}(\rho_{e\tau}) \\ -2\text{Im}(\rho_{e\tau}) \\ \rho_{ee} - \rho_{\tau\tau} \end{bmatrix}. \quad (10)$$

This is identical to the well-known Bloch vector. This representation of the polarization vector is shown in Fig. 2. Eq. (10) can also be recovered purely geometrically. Remember that $\rho_{e\tau} \in \mathbb{C}$, so it

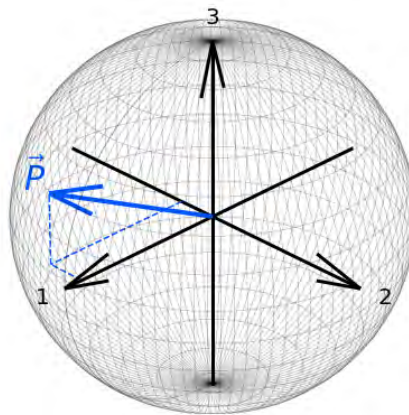


Figure 2: The polarization vector may be represented as a point on the surface of a unit sphere in a space spanned by the three Pauli matrices.

may be expressed as $\rho_{e\tau} = e^{-i\phi}|\rho_{e\tau}|$. This phase angle ϕ can be interpreted as the azimuthal angle in spherical coordinates. Therefore the x and y coordinates in this space may be interpreted as the

real and imaginary components of $\rho_{e\tau}$ respectively. After some work, one can show from the unit trace of ρ^2 that the maximum magnitude $\rho_{e\tau}$ can assume is $|\rho_{e\tau}|_{\max} = \frac{1}{2}$. However, the radius of the unit circle in the x - y plane is 1. Therefore, we should scale $x = \text{Re}(\rho_{e\tau})$ and $y = -\text{Im}(\rho_{e\tau})$ by an overall factor of two. Leaving behind the x, y, z notation in favor of 1, 2, 3 so as not to confuse these labels with any spatial directions, we can now write two components of \vec{P} as

$$P_1 = 2\text{Re}(\rho_{e\tau}) \quad \text{and} \quad P_2 = -2\text{Im}(\rho_{e\tau}). \quad (11)$$

Noting that a vector spanning the unit sphere has magnitude $|\vec{P}| = 1$, it can be shown that P_3 must be

$$P_3 = \rho_{ee} - \rho_{\tau\tau}. \quad (12)$$

This is a convenient mapping as P_3 carries useful information regarding the flavor state of the gas. When the polarization vector lies within the upper hemisphere ($P_3 > 0$), the state of the system is polarized in the electron flavor state ($\rho_{ee} > \rho_{\tau\tau}$). When the polarization vector lies within the lower hemisphere ($P_3 < 0$), the state of the system is polarized in the tau flavor state ($\rho_{\tau\tau} > \rho_{ee}$). Equation (10) defines the three components of the polarization vector \vec{P} as a natural geometric mapping from the density matrix. The rest of this work will discuss flavor dynamics using the formalism of the polarization vector \vec{P} .

In its simplest form, the equation of motion for the state of the neutrino gas expressed using \vec{P} is given as

$$(\partial_t + \hat{v} \cdot \nabla)\vec{P} = \vec{H} \times \vec{P} \quad (13)$$

where the Hamiltonian \vec{H} is the summation of vacuum, matter, and neutrino-neutrino interaction potentials

$$\vec{H} = \omega\vec{B} + \lambda\hat{e}_3 + \vec{V}_{\vec{p}}. \quad (14)$$

The term $\omega\vec{B}$ generates vacuum oscillation, where ω is the vacuum oscillation frequency and $\vec{B} = \sin(2\theta)\hat{e}_1 - \cos(2\theta)\hat{e}_3$. \vec{B} is determined by the vacuum mixing angle θ previously discussed in Section 1.1.1. The next term $\lambda\hat{e}_3$ represents the matter potential, λ is defined as $\lambda = \sqrt{2}G_F n_e$ where G_F is the Fermi coupling constant and n_e is the net electron number density. Lastly, the term $\vec{V}_{\vec{p}}$ represents the potential from neutrino-neutrino scattering. For a neutrino with momentum \vec{p} , this potential is given by

$$\vec{V}_{\vec{p}} = \sqrt{2}G_F \int \frac{d^3p'}{(2\pi)^3} (1 - \hat{v} \cdot \hat{v}') \{ [f_{\nu_e}(\vec{p}') - f_{\nu_\tau}(\vec{p}')] \vec{P}_{\vec{p}'} - [f_{\bar{\nu}_e}(\vec{p}') - f_{\bar{\nu}_\tau}(\vec{p}')] \vec{P}_{\vec{p}'} \} \quad (15)$$

where $f_{\nu_i}(\vec{p})$ is the occupation number of a neutrino or antineutrino in flavor state i with a given momentum \vec{p} . Note that this interaction depends on the intersection angles of two neutrinos, indicated by the inner product of their velocities.

It is clear that Eq. (13) will never change the magnitude of \vec{P} because its transport (the convective derivative on the left-hand side) is always perpendicular to \vec{P} . This can be seen by dotting both sides of Eq. (13) by \vec{P} and noticing that the right-hand side is zero.

2.2 The two-angle 2D line model

The self-coupled nature of the neutrino-neutrino Hamiltonian makes simulating these flavor dynamics a computationally challenging task. This problem is usually reduced to fewer dimensions in order to study its core physics. In this work we will perform additional analysis on simulations of the 2D neutrino line model which were presented by Martin, Abbar and Duan in [15]. The neutrino

line model examines a small, two-dimensional region of space with a high number density of neutrinos. In a supernova environment, we consider the emission line to lie at a radius of 100 km from the supernova so that $x, z \ll r$. That way, the angular spectrum of neutrinos passing through this region should remain constant given small changes in x and z . Additionally, the number density of neutrinos should not be expected to change very much given small changes in z . Note that in the presence of a large matter profile: $\lambda \gg \omega$. Therefore, we may work in a rotating frame about \hat{e}_3 and note that some rapidly oscillating components of \vec{B} will average to zero. This allows for the following simplification

$$\omega\vec{B} + \lambda\hat{e}_3 \longrightarrow -\eta\omega_{\text{eff}}\hat{e}_3 \quad (16)$$

where $\eta = +1$ (-1) if the normal (inverted) hierarchy is adopted, respectively and $\omega_{\text{eff}} = \omega|\cos(2\theta)|$. This change to a rotating frame about \hat{e}_3 simplifies the oscillation Hamiltonian greatly, as only the neutrino-neutrino coupling potential remains.

One spatial dimension (denoted as x) runs parallel to the surface. This axis is referred to as the emission line. This axis is periodic to enforce continuity at the boundaries. The other spatial dimension (denoted as z) is the radial distance from the spherical emission surface within the supernova. In both the two-angle and multi-angle line model, neutrinos are emitted from the emission line into the plane spanned by these two spatial dimensions. The two-flavor approximation is taken for this model, where there is only an electron neutrino and an ‘‘other’’ neutrino flavor, which we will call ν_τ .

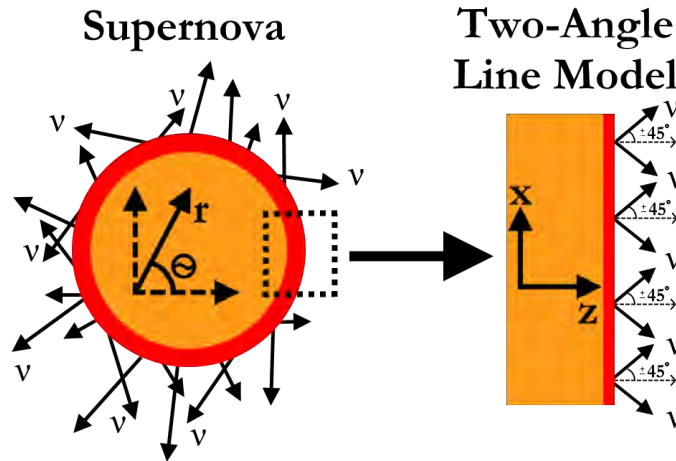


Figure 3: Comparison of the spherical geometry of a supernova to the two-dimensional Cartesian geometry of the two-angle line model. All neutrinos are emitted in beams from the flat emission plane (the x axis) at equal and opposite angles ($\pm 45^\circ$) from the z axis.

Two parameters α and μ may be tuned to probe the dynamics of dense neutrino gases with different properties. α is the ratio of number densities of antineutrinos to neutrinos

$$\alpha = \frac{n_{\bar{\nu}_e}}{n_{\nu_e}}. \quad (17)$$

The parameter μ controls the strength of the neutrino-neutrino interaction. In the two-angle line model μ may be expressed as

$$\mu = 2\sqrt{2}G_{\text{F}}n_{\nu_e}(1 - v_z^2). \quad (18)$$

The two-angle line model emits two beams of neutrinos along the emission line at angles $\Theta = \pm \frac{\pi}{4}$ from the z -axis, as shown in Figure 3. A number of conditions may be supplied that determine the

initial neutrino flavor spectrum. When this perturbation is uniform in x the neutrino gas remains correlated along x and oscillates periodically in z . This periodicity is demonstrated in Figure 4(a), which plots the probability that the gas is measured in the electron neutrino flavor state at each point in x and z . When the translational symmetry in x is broken, this spatial correlation quickly vanishes. Figure 4(b) demonstrates the flavor evolution of the gas when a sinusoidal perturbation is supplied. In the sinusoidal case, the first several kilometers in z exhibit similar behavior to the uniform perturbation until power begins to transfer to higher spatial modes of oscillation. At this point, fine scale structure begins to develop in the neutrino gas.

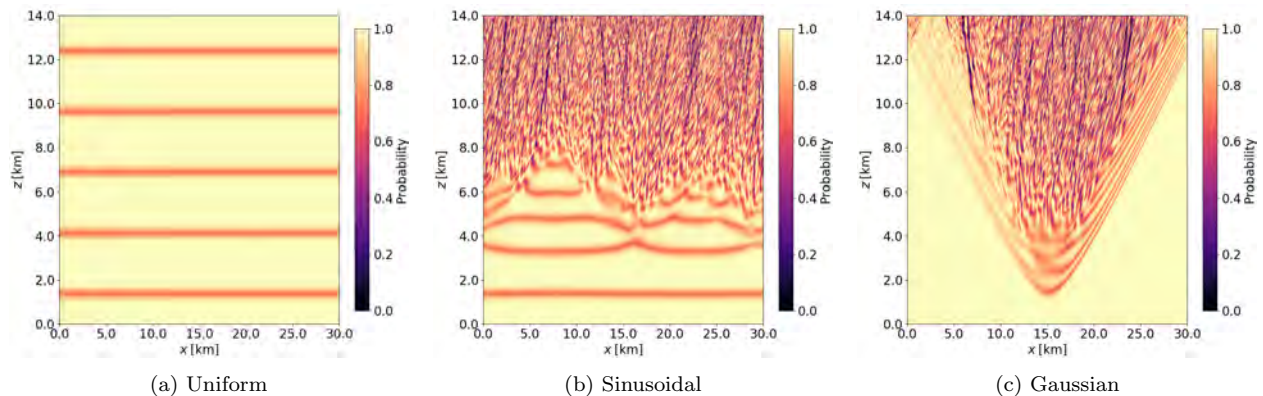


Figure 4: The electron flavor survival probability for the right-going neutrino beams shown in a heat map of x vs. z with various perturbations. The antineutrino-neutrino ratio in these calculations is $\alpha = 0.6$, the coupling strength is $\mu = 25$. Because only the right-going neutrino beams are shown, the last two figures are not symmetric. When averaged over the left and right neutrino beams, the Gaussian case would be symmetric about $x = 15$ km. The sinusoidal perturbation is antisymmetric about $x = 15$ km, so it should not be expected to appear symmetric.

Localized perturbations give rise to interesting results. Figure 4(c) demonstrates the evolution of the neutrino gas when a small Gaussian perturbation is placed in the center of the emission line. The Gaussian perturbation expands and is transported along the neutrino beam lines. Regions in x that have not yet encountered the perturbation remain in the electron flavor state. The gas develops fine structure within the core of the expanding flavor conversion region. In both cases where the translational symmetry in x is broken, the neutrino gas exhibits strikingly similar behavior within the non-linear regime despite coming from distinct perturbation profiles. Recently, it was discovered that the average flavor content of the gas saturates to the same value in both the sinusoidal and Gaussian calculations, provided other parameters are identical [15]. A comparison of this saturation behavior between sinusoidal and Gaussian initial conditions is provided in Fig. 5.

The behavior of the neutrino gas at large radii is also not strongly dependent on the amplitude of the initial perturbation, although this is not as well understood. In Section 2.4 we will discuss one of the apparent shortcomings of the two-angle line model, localized unitarity violation. Nonetheless, this simple model has provided us with useful methods for characterizing the behaviors of dense neutrino gases.

2.3 Unitarity of the polarization vector

The previous section motivated the use of polarization vector formalism by presenting it as a geometric representation of the state of the neutrino gas. This mapping disguises one constraint, the unitary summation of measurement probabilities for a system in a pure state, in the unit length

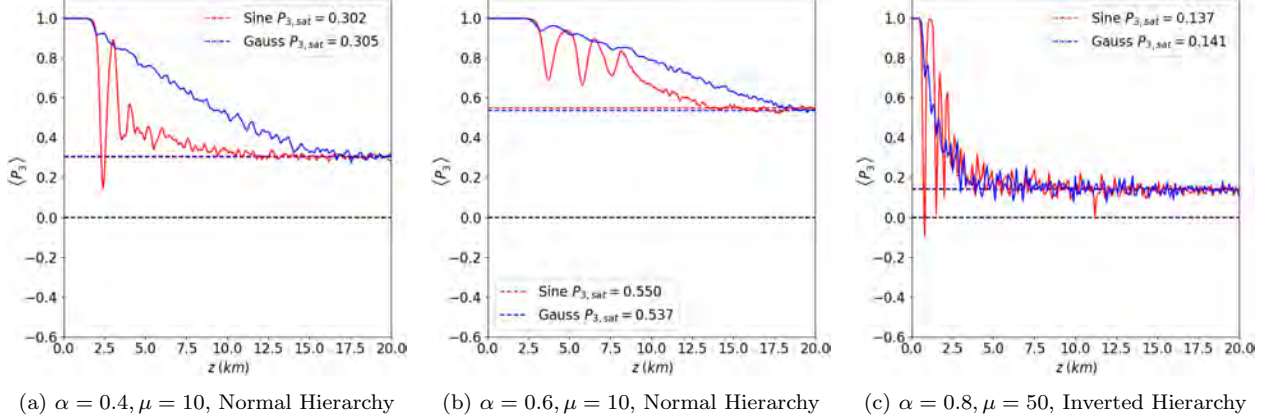


Figure 5: P_3 averaged over x , plotted along z . Each plot shows various calculations with different interaction strengths μ , antineutrino/neutrino ratios α , and mass hierarchies. Most importantly, calculations using both sinusoidal and Gaussian initial conditions are compared. Note that in either case, the flavor content of the neutrino gas saturates to approximately the same value (indicated by the dotted lines).

of the polarization vector. A brief proof using the form of \vec{P} provided in Eq. (10) that $|\vec{P}| = 1$ will now be provided. First, compute the sum of the squares of each of the three elements

$$|\vec{P}|^2 = (2\text{Re}(\rho_{e\tau}))^2 + (-2\text{Im}(\rho_{e\tau}))^2 + (\rho_{ee} - \rho_{\tau\tau})^2. \quad (19)$$

When simplified, this expression may be written as

$$|\vec{P}|^2 = -4(\rho_{ee}\rho_{\tau\tau} - \rho_{e\tau}\rho_{e\tau}^*) + (\rho_{ee} + \rho_{\tau\tau})^2. \quad (20)$$

The first term is immediately recognized as the determinant of ρ , whereas the second term is the square of the trace of ρ and must be equal to one. Remember that ρ is idempotent i.e. $\rho = \rho^2$. The determinant of any idempotent matrix that is not the identity matrix is zero. Considering this, we may now write

$$|\vec{P}|^2 = -4(0) + (1)^2 = 1. \quad (21)$$

Therefore the proof is complete. Taking the square root of both sides, we have derived the unit length of the polarization vector

$$|\vec{P}| = 1. \quad (22)$$

As the neutrino gas develops, this length should always be preserved. Viewed geometrically, the state of the system must develop in a way such that the polarization vector is constrained to the surface of the unit sphere.

2.4 Unitarity violation

Unitarity is conserved when Eq. (13) is solved exactly. However, numerical solutions will not necessarily respect this constraint if it is not explicitly enforced. As the neutrino gas evolves along the beam lines in our simulation, each step slightly adjusts the magnitude of the polarization vector and violates this constraint. In the direction of increasing radius (along z) this violation grows slowly across x . This deviation provides a useful estimation for the global accumulation of numerical error in our simulation. We stop our simulation when $||\vec{P}| - 1| \approx 10^{-2}$, i.e. unitarity is

violated on the order of 1%. Not only do we stop the simulation because the results are becoming increasingly nonphysical, but also due to practical computational limitations. Our numerical solver takes dynamic step sizes based on the approximate error generated by each step. When this error grows too large, the step size plummets and the simulation comes to a near halt.

When the neutrino gas begins to develop small-scale structure in the two-angle line model, small regions of the neutrino gas undergo flavor oscillation at very short distance scales in x . When the scale of this oscillation approaches the spatial resolution of the simulation, these regions develop unitarity violation much more quickly than others at the same radius. These intense and localized peaks in unitarity violation are transported along the beam lines and brought in contact with the rest of the neutrino gas. These localized peaks grow much more quickly than the rise of global numerical error. In any case where the neutrino gas develops small-scale structure, this effect always stops the simulation. An example of this rapid growth is pictured below in Fig. 6:

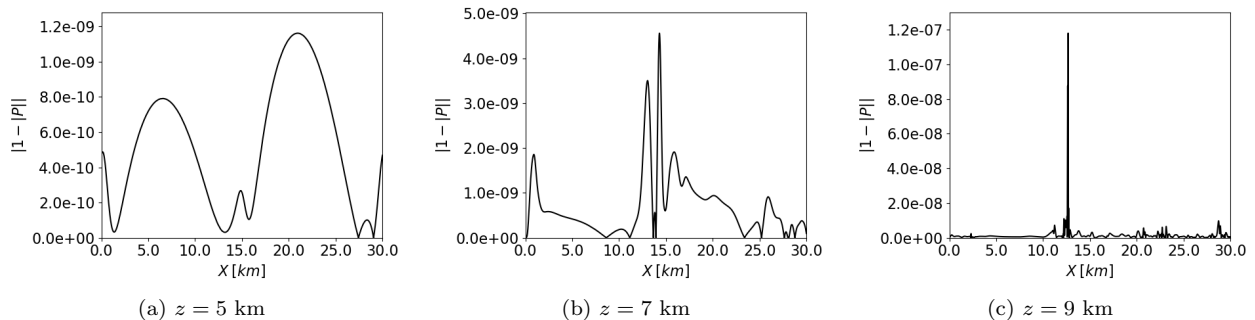


Figure 6: Some regions develop localized patches of unitarity violation very quickly. Here, three radial snapshots of the unitarity violation along x are shown. This is a sinusoidal perturbation with $\mu = 10$ and $\alpha = 0.5$.

In Fig. 6(a) at 5 km, there are no discernible sharp peaks, just two wide lobes with a small feature in the center. In Fig. 6(b) at 7 km, that central sharp feature has grown by more than an order of magnitude. By 9 km in Fig. 6(c), this feature has grown by almost another two orders of magnitude. Just a few kilometers after its first appearance, this peak completely dwarfs global unitarity violation. At larger radii, more peaks eventually grow that may even outpace some of the first few to appear. Eventually, there are a small handful of peaks that drive up the numerical error of the simulation far above the global average.

3 Addressing Fine Structure

In the two-angle line model, regions of the neutrino gas develop fine structures that strongly violate the unitarity of the polarization vector. Ref. [15] demonstrates that the coupling of Fourier modes in the two-angle line model are responsible for transferring power from large-scale structure to smaller scales, however it remains to be seen whether the development fine structure is a general feature of most dense neutrino gases. In either case, it is untenable to perpetually increase the spatial resolution of our simulation as structures in the neutrino gas continue to develop at smaller scales. This section explores a few methods for addressing this issue, as well as future computational possibilities for simulating dense neutrino gases.

First, we discuss early attempts to smooth fine structure that develops in the neutrino gas by interpolating elements of the polarization vector individually. Second, we introduce a refined definition of fine structure founded on the unit sphere i.e. “angular dispersion”. Third, we present

methods for interpolating the polarization that leverage the geometry of the unit sphere and discuss the computational opportunities these methods could offer. Fourth and finally, we introduce the multi-angle line model and discuss early results that could make it a promising candidate to succeed the two-angle line model.

3.1 Element-wise interpolation of the polarization vector

We can artificially impose a minimum scale of fine structure permitted to develop within the neutrino gas by smoothing fast-oscillating regions when they appear. This is a delicate process. Once higher modes in the spectrum of the neutrino gas are activated, they cannot simply be removed from the spectrum. Outright removing higher oscillation modes would violate unitarity strongly, as those modes would be in different phases at different spatial points in the neutrino gas.

Early attempts at smoothing fine structure in the neutrino gas involved coarse interpolation of the individual polarization vector elements to broader their scale of oscillation. Unfortunately, no standard interpolation methods provided results that satisfied the unitarity constraint and eliminated fine scale structure simultaneously. Below in Fig. 7 we illustrate the results of one characteristic attempt to smooth fast oscillation using a standard cubic coarse spline for each polarization vector element. Coarse splines involve sampling data at large intervals. However, if this interval is too large the interpolant for each polarization vector element will violate unitarity even more severely than the original data. There are no ways to constrain independent splines, so each interpolant does not know to adjust with respect to the others to respect unitarity. Therefore this sampling interval needs to be quite small, on the order of several x bins. Once data is too finely sampled, interpolation can only produce results that look very similar to the original data. There is no satisfactory “middle ground” for sampling intervals that works well for all unitarity violating regions, so this method will not be effective for automatically smoothing fine structure.

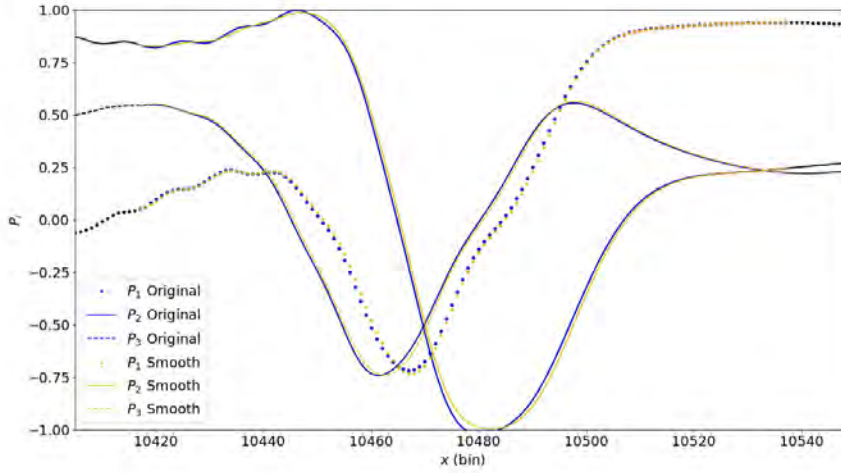
3.2 Angular dispersion on the unit sphere

Recall the representation of the polarization vector as a point on the surface of the unit sphere. One can view the evolution of the entire gas by viewing every polarization vector for all values of x at a given radius for a given radius. This is done in Fig. 8 with snapshots at several radii.

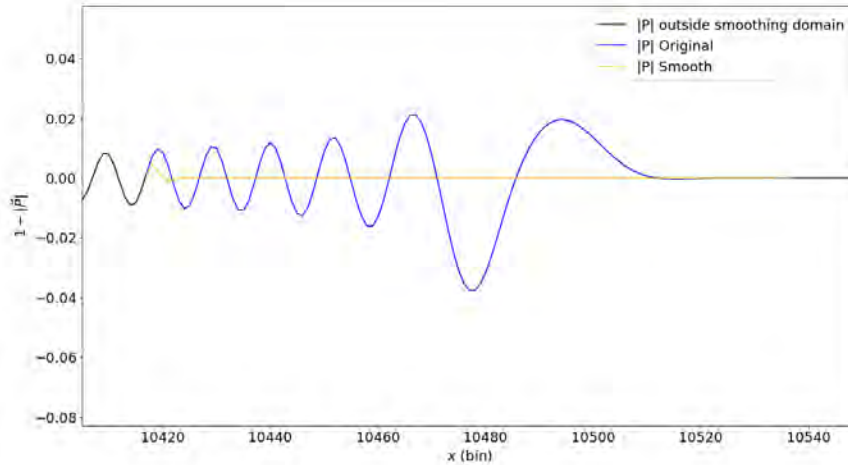
At large radii, one can see that the polarization vectors within a unitarity violating region follow a long and winding path over the surface of the unit sphere. In retrospect, this behavior makes sense. If the flavor state of the neutrino gas undergoes rapid oscillation at the scale of several x bins, it will appear as though the polarization vector is whipping rapidly around the unit sphere. In addition, each of these points on the unit sphere will be separated far apart from one another. Alternatively, well sampled oscillation at longer distance scales will be better resolved and forms a continuous line over the surface of the unit sphere instead.

We will take a brief aside to define a quantity named angular dispersion, and will then return to the interpolation problem. The angular dispersion of these points, defined in Eq. (23) as the left-right averaged angular separation of the polarization vectors from neighboring x -values, characterizes this sampling problem for trajectories on the unit sphere. Angular dispersion is high in regions with very rapid oscillation that cannot be sampled sufficiently by the spatial resolution of the simulation. The definition of angular dispersion follows directly from the definition of the cosine of the angle between two vectors

$$\Delta\Theta(x_i, z) = \frac{1}{2} \left[\arccos \left(\frac{\vec{P}(x_i, z) \cdot \vec{P}(x_{i+1}, z)}{|\vec{P}(x_i, z)| |\vec{P}(x_{i+1}, z)|} \right) + \arccos \left(\frac{\vec{P}(x_i, z) \cdot \vec{P}(x_{i-1}, z)}{|\vec{P}(x_i, z)| |\vec{P}(x_{i-1}, z)|} \right) \right]. \quad (23)$$



(a) All three elements of the polarization vector shown, original values shown in blue while “smoothed” values are shown in orange. Because this method attempts to maintain the approximate shape of each polarization vector element while enforcing unitarity, all elements remain nearly unchanged.



(b) Violation of unitarity before and after the smoothing operation. This method succeeds in reducing the magnitude of unitarity violation, but because fine structure is still present this can only be a temporary fix.

Figure 7: Cubic spline interpolation of \vec{P} .

Note that this angle does not correspond to rotation about any one particular axis. It represents the average of two rotation angles that could very well be about two different axes. Returning to the issue of regions with fine structure oscillation and interpolation, we note that this is the equivalent to discussing regions with high angular dispersion. We have expanded the definition of fine structure to include rapid oscillation about any axis on the unit sphere. These regions have very high angular dispersion and thus follow lengthy trajectories over the surface of the unit sphere. In some cases, the polarization vector will wrap around the sphere multiple times over the span of a few dozen x -bins, whereas a low-angular dispersion region could take hundreds of x -bins to

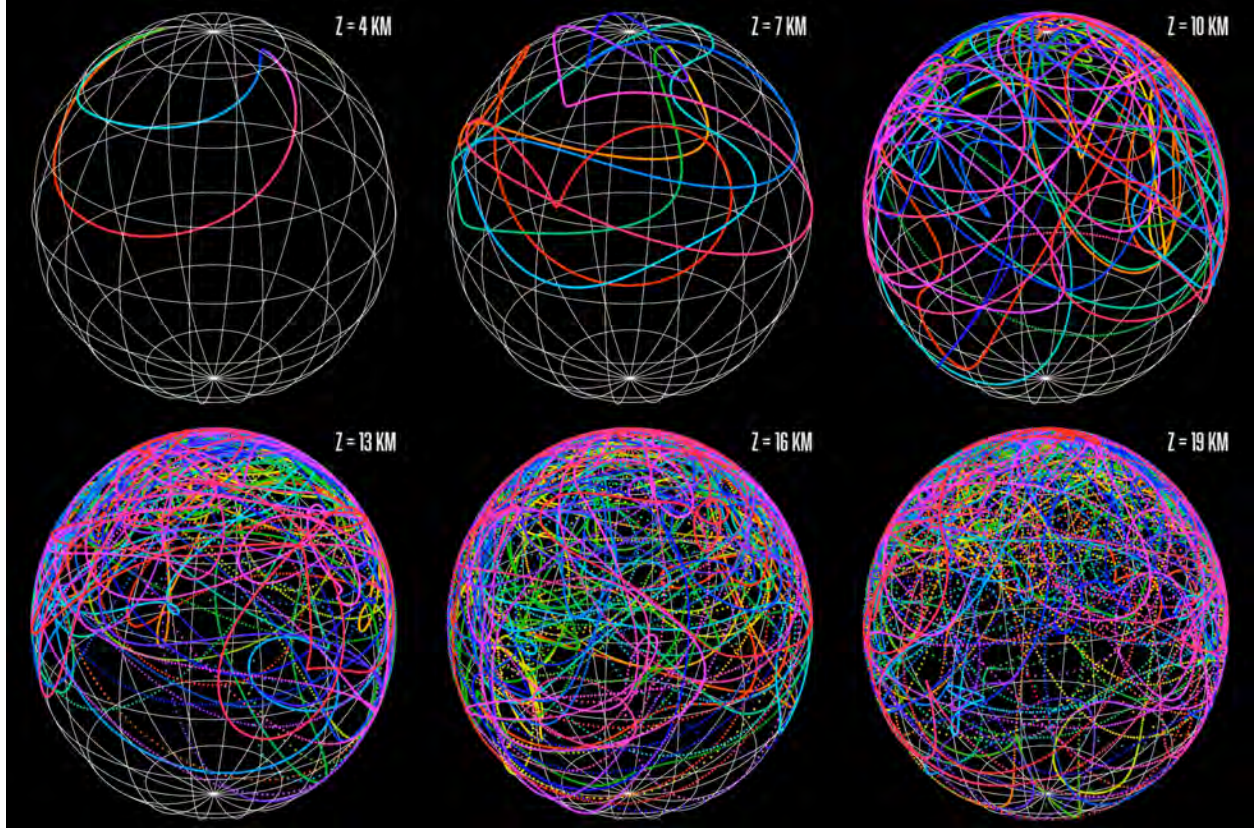


Figure 8: Snapshots of the developing neutrino gas at various radii represented on the unit sphere. Each point is colored by its spatial position in x . Points for all values of x are shown. At small radii, the trajectory resembles a short loop of string resting on the surface of the sphere. At larger radii, this loop of string is stretched out over the unit sphere many times. Extreme examples of this stretching can be seen in regions where individual points are visible. These regions have high angular dispersion.

complete a single rotation. One can observe the relationship between high angular dispersion and unitarity violation directly on the unit sphere as shown in Fig. 9. However, it is more informative to watch high angular dispersion regions develop along increasing radii and note the rapid increase in unitarity violation at those points. This is demonstrated in Fig. 10.

Interpolating these trajectories in a way that represents the original trajectory while preserving unitarity *and* smoothing fine structure is an impossible task. There are no trajectories that could follow attempt to follow the complete path taken in this region while shortening it dramatically. The spherical geometry that constrains unitarity fundamentally constrains the possible paths. Any interpolation attempt that does not violate unitarity as egregiously as the original data will follow a very similar path to that of the original data set. Even if it momentarily fixes the violation of unitarity, it retains the high angular dispersion that could not be sampled accurately by the numerical simulation and generated extreme unitarity violation. Therefore, element-wise interpolation of this region only disguises the rise of numerical error.

Element-wise interpolation failed because it did not utilize the information freely offered to it by the geometry of the unit sphere. It is impossible to respect the fundamental constraints of the polarization vector while drawing short trajectories that mimic the original data. The best

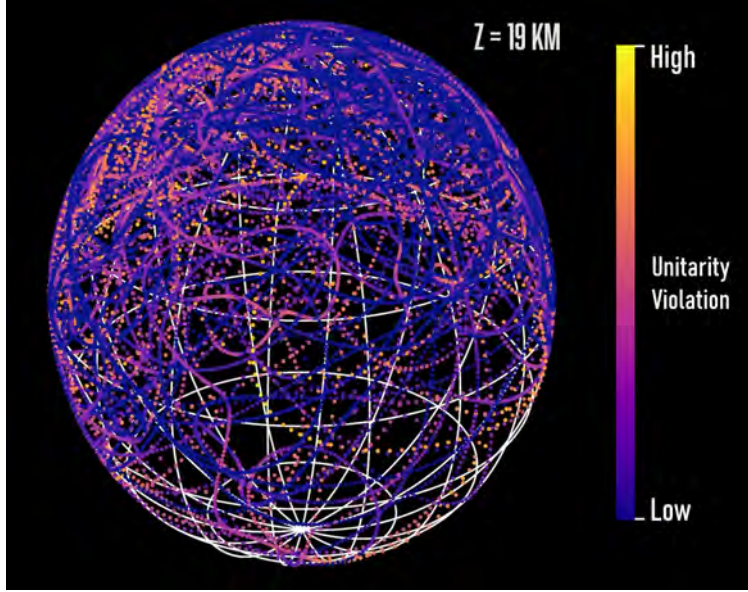


Figure 9: Snapshot of the trajectory of the neutrino gas along all x at $z = 19$ km. The color scale indicates magnitude of unitarity violation. Note that neighboring points that are spaced further apart are often more brightly colored than closely resolved trajectories that still look like continuous lines.

resolution to this fine structure problem embraces this geometric constraint and offers a number of compelling solutions.

3.3 Fine structure smoothing — spherical interpolation

The element-wise solution for smoothing fine structure oscillation in P_3 failed because it is impossible to meet each of the three main demands: unitarity, short trajectories, and similarity. Unitarity preservation is a fundamental constraint, therefore it should not be challenged. Additionally, we should not create any more winding trajectories over the unit sphere. Similarity between the adjusted trajectory and the original trajectory of the polarization vector must be compromised if there is any hope for a viable trajectory.

The previous perspective was that we should coarsely interpolate each element of the polarization vector and then consider how it affected the trajectory over the unit sphere. Now approach this in the reverse order. The only productive solution is to first consider the shortest paths between the boundaries of this unitarity-violating region, and then consider this trajectory's effect on each element of \vec{P} . Imagine a scenario where a region in the neutrino gas has high dispersion, and it quickly wraps once around the unit sphere before slowing down again close to the point where it had started to speed up in the first place. The points on the boundary of this region lie much closer to one another than the length of the trajectory that connects them. One could connect these points with a much shorter trajectory than the one it takes in the same number of steps. We will now discuss two methods to generate these trajectories. The main takeaway from this section, however, is the realization that the preservation of the original form of these high angular dispersion paths must be sacrificed in order to smooth out fine structure.

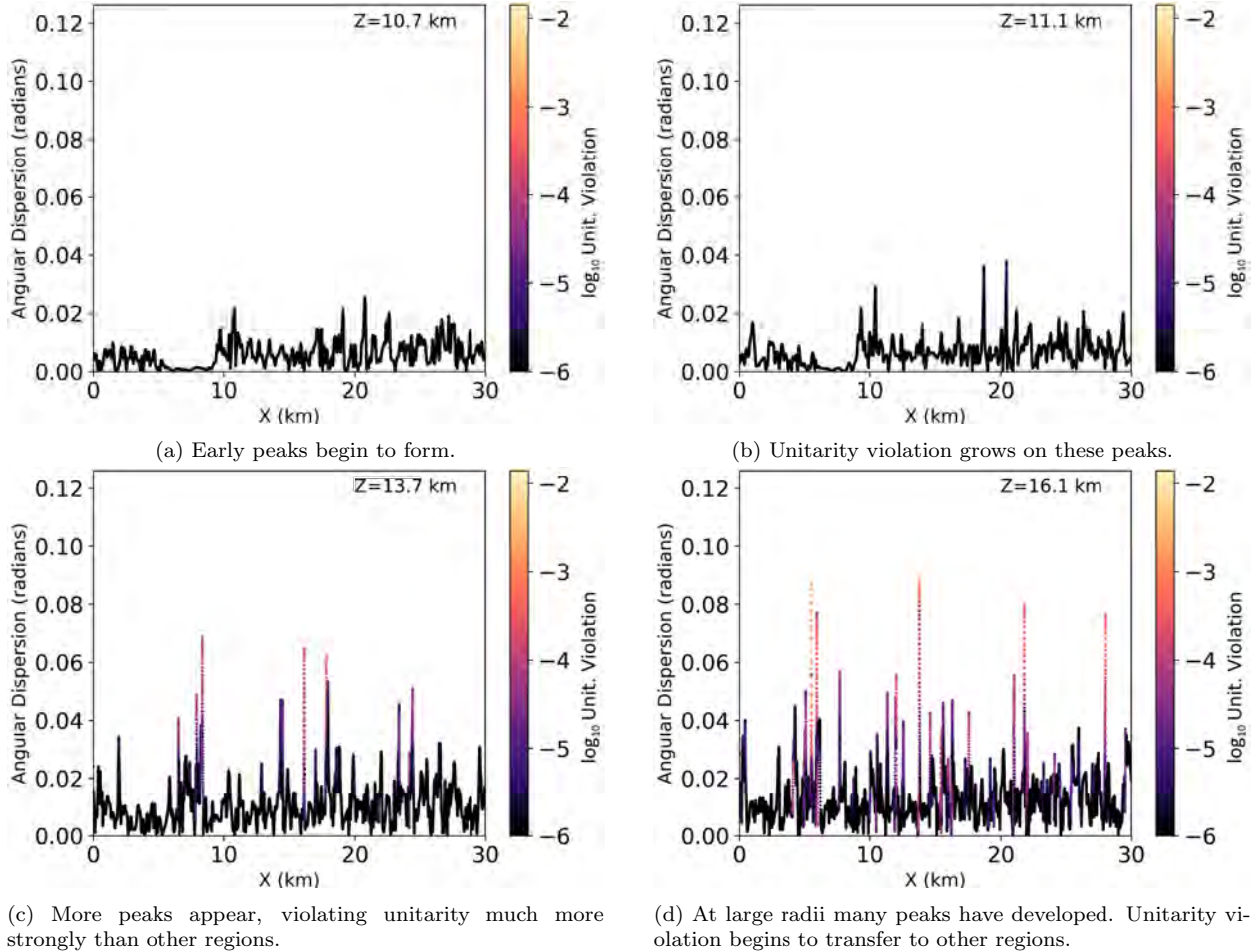


Figure 10: Snapshots of angular dispersion along x for various radii (z). Thin peaks in angular dispersion appear, continue to grow and eventually develop strong unitarity violation. Once enough of these peaks appear, unitarity violation begins to transfer to other regions of the neutrino gas with lower angular dispersion.

3.3.1 Geodesics

The shortest and easiest way to connect these two points is to connect them by their great circle. On the surface of a sphere, the great circle that connects two points represents their geodesic, the minimized path given some constraint of motion. This trajectory will remain on the surface of the unit sphere therefore it satisfies the unitarity constraint. An example of a great circle geodesic connecting the boundaries of a high angular dispersion region is shown below in Fig. 11. Note that the angular dispersion of the points along the great circle trajectory is not even visible by eye. A comparison of the violation of unitarity before and after geodesic interpolation within this region is provided by Fig.12(b), whereas the effect on the individual polarization elements can be seen in Fig.12(a).

Computing great circle trajectories is a straightforward computational task. In principle, one must only identify the axis of rotation between these two points. With this axis, one can vary the angle of rotation between zero and the angular separation between the points to generate the trajectory. The efficiency of this calculation further improves when quaternion representations

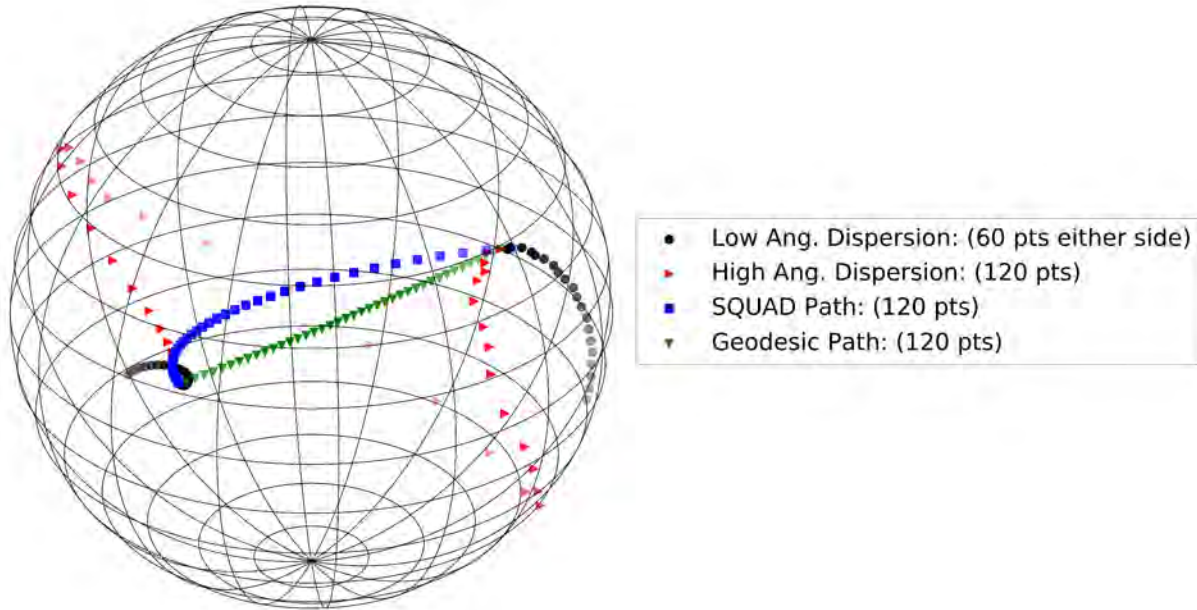


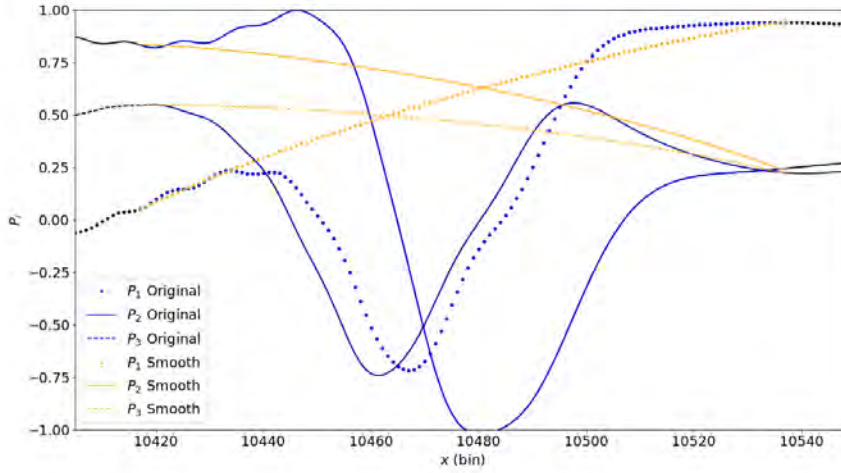
Figure 11: Comparison of two trajectories over the unit sphere that connect the boundaries of the high angular dispersion regime (shown in red). The great circle geodesic (shown in green) connects these two boundary points in the shortest path possible, although it has a kink at the leftmost boundary. The trajectory drawn by Squad (shown in blue) takes a slightly longer trajectory but it captures the behavior outside this region (the black dots) and has no kink discontinuities.

of rotations are used. Linear interpolation of quaternions, often called a *Slerp* [16], can generate discrete points along this great-circle trajectory. Quaternions and their applications to interpolating rotations will be discussed in much greater detail in the next section.

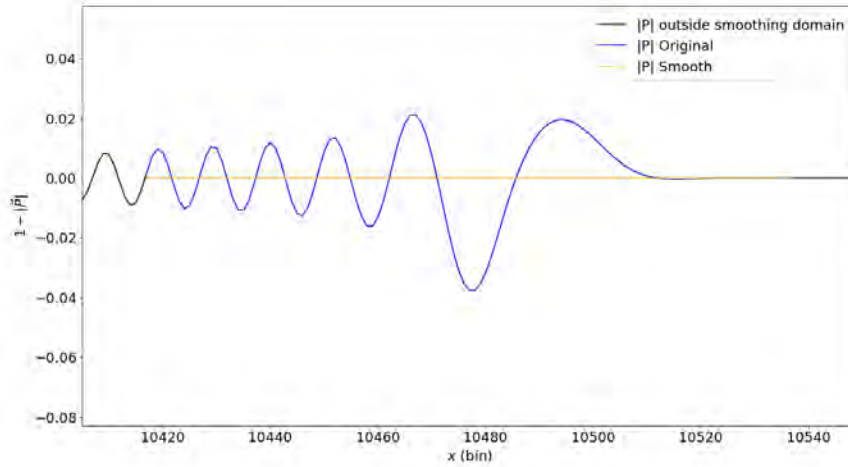
Great circles will not capture any behaviors of the neutrino gas inside or even outside this smoothing region. Discarding internal information is an intentional part of this smoothing process, however it cannot differentiably connect to the boundaries of this region. This leads to kink discontinuities, where the direction of the great circle trajectory does not continuously transition to the polarization vectors outside this smoothing region. An example of this can be seen at the leftmost boundary of the blue trajectory shown in Fig. 11. Kink discontinuities will likely present a problem for the numerical simulation. If these kinks are well-resolved by many points, this feature will not be as sharp as it appears to be on the neutrino gas when viewed along x instead. Nonetheless, while the great circle may represent the shortest trajectory, it will always be the most crude and unnatural replacement.

3.3.2 Quaternion interpolation and Squad

The late 20th century witnessed a rapid development of computer graphics. Not only did computer hardware improve exponentially year after year, but also did the sophistication of mathematical methods used to perform common operations. Smooth interpolation between rotations on the surface of a sphere is a challenging problem to solve using traditional representations of rotations. These tools were designed for discrete operations that follow a particular order. Suddenly in the 1980's, an obscure representation of rotations from pure mathematics and physics resurfaced: quaternions. Originally presented in 1843 by William Hamilton, quaternions were designed to



(a) All three elements of the polarization vector shown, original values shown in blue while smoothed values are shown in orange. Each polarization vector element is changed dramatically because the sharp oscillation feature within them has vanished.



(b) Violation of unitarity before and after the smoothing operation. This method should be and is successful at reducing unitarity violation as the geodesic is constrained to the surface of the unit sphere.

Figure 12: Geodesic interpolation of \vec{P} .

allow the computation of the quotient between two vectors in three dimensional space. Their most straightforward definition is

$$q = a + bi + cj + dk \quad (24)$$

Where i, j, k can all be considered as distinct imaginary units, similar to the appearance of i in the representation of a complex number $z = a + bi$. The square of each of these imaginary units is equal to -1 . The multiplication algebra of these units is non-commutative, following a particular handedness. For example, circular permutations of a product of these units leave the sign of the

product unchanged

$$ij = k, jk = i, ki = j \quad (25)$$

However, exchange of any two units in a product changes the sign of that product

$$ji = -k, kj = -i, ik = -j \quad (26)$$

Quaternions are strange algebraic objects that are often difficult to understand intuitively. However, they hold great utility for algebraic representation of rotations in three-dimensional space since they compactly represent general rotations in a computationally efficient algebraic form. Quaternions are commonly used today in 3D computer graphics and robotics for this reason.

We want to smoothly interpolate series of rotations to correct high angular dispersion trajectories on the unit sphere. Generally, interpolation curves that pass through every control point adjust the first derivative of the curve before it reaches the next point so that it may smoothly transition to the point after. In a sense, the curve *predicts* where the future control points are, even though the curve is not approaching these points at that time. On the surface of the unit sphere, this corresponds to a series of rotations that both reach every control point and predicts where the following points lie. While this is an impossible task with rotation matrices or Euler angles as the axis of rotation changes from one “keyframe”¹ to the next, this is easily achieved through quaternion interpolation.

The simplest form of unit quaternion interpolation is the Slerp [16], spherical linear interpolation. Slerp linearly interpolates two unit quaternions, i.e. two subsequent rotations. Previously, we discussed the use of a Slerp as a method to generate keyframes of a single rotation for a great-circle trajectory. In this case, one of the unit quaternions is the “identity” quaternion $q_{\text{ident}} = 1$. This “identity” quaternion corresponds to no rotation. Therefore a Slerp that interpolates the identity quaternion and some other arbitrary unit quaternion q will generate keyframes for the rotation represented by q . Generally, the definition of a Slerp between two unit quaternions q_0, q_1 as a function of the normalized keyframe time $t \in [0, 1]$ is

$$\text{Slerp}(q_0, q_1, t) = q_0(q_0^{-1}q_1)^t. \quad (27)$$

This is a deceptively simple definition. It is critical to note that quaternion multiplication is not generally commutative, therefore quaternion exponentiation cannot be compared to the usual scalar exponentiation. Exponentiation of quaternions is described by Ref. [17]. A quaternion may be represented by a scalar and a vector component, i.e. $q = a + [b, c, d] = (a, \vec{v})$. In this form, the product of two quaternions q_0, q_1 is defined as

$$q_0q_1 = (a_1, \vec{v}_1)(a_2, \vec{v}_2) = (a_1a_2 - \vec{v}_1 \cdot \vec{v}_2, a_1\vec{v}_2 + a_2\vec{v}_1 + \vec{v}_1 \times \vec{v}_2) \quad (28)$$

whereas the inverse q^{-1} of a quaternion q is defined as

$$q^{-1} = \frac{(a, \vec{v})}{a^2 + |\vec{v}|^2}. \quad (29)$$

Something worth a quick note is that we used Slerp to interpolate the “identity” quaternion q_{ident} and q to generate a great circle connecting two points on a 3-dimensional unit sphere. However, the use of Slerp for any pair of unit quaternions will also connect these quaternions via a “great circle” on a 4-dimensional sphere of unit quaternions. This simple step clarifies the mechanics of quaternion interpolation, and reveals that this is actually very similar to our original problem

¹keyframes represent discrete steps that compose a complete rotation

of smoothly connecting points in 3-dimensional space. Quaternion interpolation simply draws trajectories connecting control quaternions in this higher 4-dimensional space of quaternions. With this in mind, it is clear that many solutions for the interpolation of any number of rotations are possible.

This brings us to Squad, otherwise known as spherical quadrangle interpolation. This method was also developed by Shoemake in the late 1980’s and is examined in [17]. Squad can interpolate between an unlimited series of rotations represented by unit quaternions. Aside from being very computationally efficient, it is also defined in a relatively straightforward manner. A Squad is the combination of multiple Slerps using what are referred to as helper quaternions to define the vertices of a “quadrangle”. Squad for two control quaternions q_i, q_{i+1} and two helper quaternions s_i, s_{i+1} at a normalized keyframe time $t \in [0, 1]$ is defined as

$$\text{Squad}(q_i, q_{i+1}, s_i, s_{i+1}, t) = \text{Slerp}(\text{Slerp}(q_i, q_{i+1}, t), \text{Slerp}(s_i, s_{i+1}, t), 2t(1 - t)). \quad (30)$$

The helper quaternions s_i and s_{i+1} are defined recursively based on the control quaternions q_{i-1}, q_i, q_{i+1} , and q_{i+2} . These helper quaternions provide information about past, present, and future rotations to the interpolation curve. This recreates the characteristic “predictive” behavior of smooth interpolations.

Overall, Squad produces visually pleasing trajectories with reasonable angular dispersion between each pair of key frames. Figure 11 demonstrates Squad being applied to one of these high angular dispersion regions. Compared with the geodesic trajectory, Squad joins at the boundary much more smoothly. Additionally, the angular dispersion of the Squad trajectory is not necessarily constant whereas the great circle outputs key frames at equal angular intervals. Note that both external trajectories on the left and right represent 60 points each, although the right trajectory is longer because it has a higher angular dispersion than that of the one on the left. Squad notices this discrepancy and gradually increases its angular dispersion as it moves from left to right (Note that the line becomes lighter as it moves to the right because the points are spaced further apart). While the angular dispersion is still not perfectly continuous at the boundaries, it is a far more natural solution than one where a constant angular dispersion is enforced.

3.4 Outlook for fine structure smoothing

In this section we reframed the problem of rapid flavor oscillation in the neutrino gas into general fine structure such as rapid rotation about the unit sphere. We originally suspected that rapid oscillation of the flavor content of the neutrino gas (characterized by P_3) was solely responsible for this issue of unitarity violation. By viewing a series of neighboring polarization vectors as trajectories across the unit sphere, we noticed that this issue actually stems from rapid rotation around the unit sphere about any axis. This means that rapid oscillation of both the flavor content of the gas and the quantum coherence between these flavor states contribute to the rapid growth of unitarity violation. This geometric perspective also shed light on possible solutions to this problem. We explored two possibilities for smoothing fine structure in the neutrino gas by drawing shorter trajectories over the unit sphere than those originally followed. Geodesics offered the shortest and simplest replacement trajectory, whereas Squad offered more a natural replacement trajectory based on an interpolated sequence of rotations.

Implementing one of these trajectories or others that decrease angular dispersion and maintains unitarity is a promising solution for managing the rapid rise of intense and localized violations of unitarity. As previously discussed, the algorithm for our numerical solver takes dynamic step sizes. When numerical error grows too large, these step sizes shrink rapidly until the solver is no longer making any meaningful progress. So far, all large numerical error in the form of unitarity

violation is due to these few localized regions that developed fine structure. If these points were to be smoothed out before they develop high numerical error, the two-angle line model calculations could progress much further.

Currently, we have not implemented a smoothing solution within the two-angle line model calculation so it is not possible to examine the physical effects this algorithm may have on the development of the neutrino gas. It seems reasonable to suspect that smoothing a few dozen points out of tens of thousands at smaller radii would not hold any dramatic future consequences for the long-term behavior of the neutrino gas. However, at large radii the algorithm would start to smooth very large regions of the neutrino gas as more regions develop small scale structure. Therefore, this method of smoothing sets a lower bound on the scale of structures permitted to form in the gas. If the neutrino gas continues to develop smaller scale oscillation without limit as the radius increases, this lower bound on structure scale can only impose a new maximum radius the calculation can reach before this algorithm is artificially adjusting the entire neutrino gas. However, it is unclear when this limit would be reached and it seems that the implementation of this correction algorithm would let us reach much larger radii before needing to stop the calculation once again.

3.5 The multi-angle 2D line model

An alternative to fine structure smoothing is adopting a new numerical model of the dense neutrino gas. The multi-angle line model emits neutrino beams at a spectrum of angles instead of just two at each point along the emission line. This change is summarized by Fig. 13. The multi-angle model introduces a large variety of intersection angles between beams, influencing their interaction strengths. This is a more realistic model, as neutrinos should be emitted at all angles from a spherical surface within the supernova. This dispenses with the immense angular granularity imposed by the two-angle model. However, it is computationally challenging to increase angular resolution while retaining the same spatial resolution attainable by the two-angle model. We

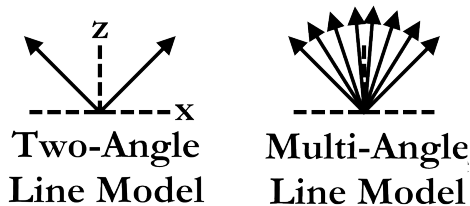


Figure 13: Schematic comparison of the two-angle and multi-angle line model.

have used several pilot calculations using the multi-angle line model performed by Martin, J.D. and Huaiyu Duan, unpublished results. These preliminary calculations have presented interesting results. Notably, the flavor content of the neutrino gas does not completely saturate at large radii. However, Fig. 14 does show that the flavor content of the neutrino gas averaged over all beams oscillates with a relatively small amplitude around a constant value. This requires further review, but this behavior bears some similarities to the saturation behavior of the two-angle line model described by Ref. [15].

Additionally, the flavor oscillation of the neutrino gas does not develop fine structure up to $z = 10$ km. So far, this is the maximum radius reached by these early multi-angle calculations because they are computationally expensive. It is unclear why increasing the variety of neutrino interaction strengths (from the numerous beam intersection angles) prevents fine structure from developing in the gas. Aspects of this fine structure problem have been investigated in the two-angle [18] and multi-angle case [19]. It is not clear why power does not transfer to higher oscillation

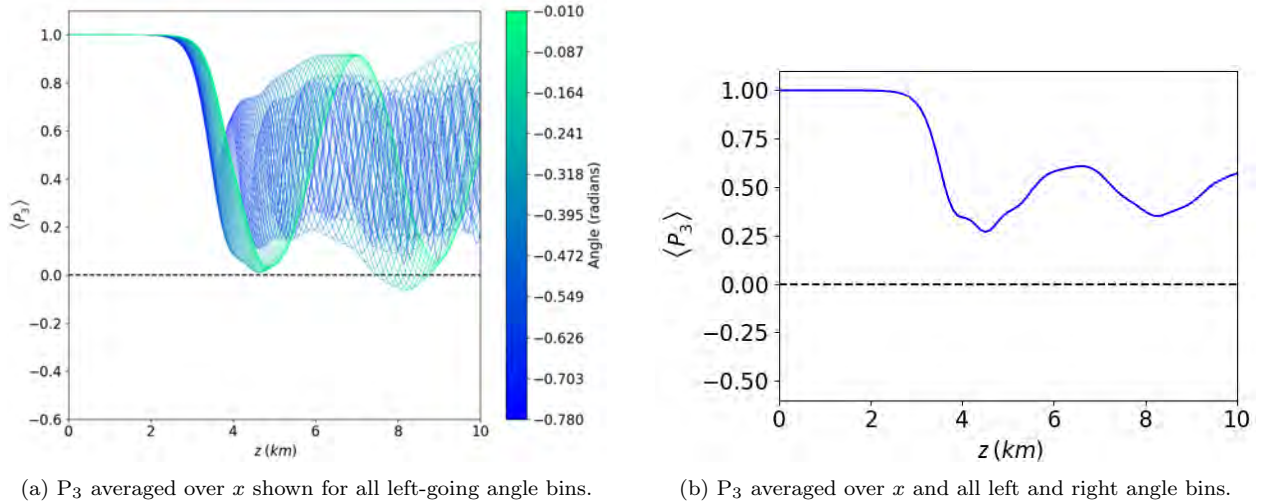


Figure 14: (Left) At large radii, the ‘DC’ offset for each angle bin is very similar. Each beam’s amplitude of oscillation is strongly dependent on its angle, decreasing as the neutrino beams become more parallel to x . (Right) When averaged over all angle bins, the oscillation about the offset persists. This behavior bears some resemblance to flavor saturation in the two-angle line model.

modes in the multi-angle line model as quickly as it did in the two-angle line model. Further analysis should be performed to determine if the development of fine structure is a general feature in these neutrino gases and if it should be expected in this multi-angle line model. For now, it remains to be seen whether the neutrino gas will eventually leave this regime of correlated oscillation and devolve into chaotic fine structure, or continue correlated oscillation about the “saturation” point indefinitely.

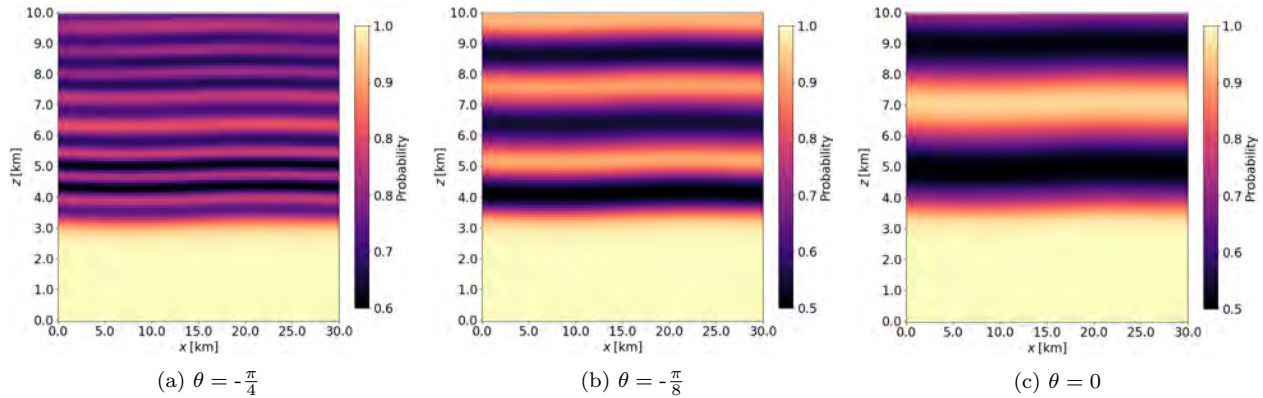


Figure 15: The electron flavor survival probability shown in a heat map of x vs. z for different angle bins in the multi-angle line model with $\alpha = 0.6$, $\mu = 10$, and a sinusoidal perturbation at $z = 0$.

The multi-angle line model is a promising model that deserves future analysis. It serves as a natural extension of the two-angle line model that is seemingly freed of fine structure that generates numerical errors such as unitarity violation, the two-angle line model’s most dire constraint. It is still more computationally accessible than the fully-realized spherical geometry of a supernova with non-trivial angular and energetic spectra, while also potentially providing the kind of unique insight

originally offered by the two-angle line model.

4 Conclusions

The line model is a computationally tractable approximation of a small, two-dimensional region of space within a core collapse supernova. We have explored geometrically-founded error correction methods for the two-angle line model that could stem the localized development of numerical error and unitarity violation. Alternatively, our preliminary analysis of the multi-angle line model suggests that it is a viable next step in numerical simulations of these gases. Although the multi-angle line model is more computationally expensive, it does not seem to develop the same fine structure in the neutrino gas that has proven to be problematic for the two-angle line model. Further work should be done to characterize these numerical models to construct a complete picture of neutrino flavor dynamics in core-collapse supernovae.

Acknowledgements

I would like to thank my advisor Dr. Huaiyu Duan and Dr. Joshua Martin for their guidance throughout this work. I have grown immensely in my confidence and abilities as a physicist over just the short year and a half I have worked on this project. One of my fondest memories of this time was the quantum mechanics crash course Josh gave me over junior year. It was empowering to build up those skills and begin to understand the work we were doing. I was dazzled by the intersection of particle physics and astrophysics our work sits at, and began to ask my own questions and set the course for my honors thesis. It was liberating to pursue each avenue that came up throughout this process while being encouraged to make my research my own. I have learned so much from this time, thank you both for the opportunity to work in NuCO. This work was supported by the Rayburn Reaching Up Fund and DOE NP grant DE-SC0017803.

As this marks the conclusion of my time at UNM, I would like to briefly give thanks to the figures who have helped me along this journey. Thanks to Dr. Dunlap for being a wonderful general physics professor, SPS advisor, renowned demo show director, and my first research advisor. SPS has always been an environment where I felt encouraged and empowered to find a place in the physics community. Thank you all for the fun meetings, long road trips to conferences, and close friendships built. It was an honor to help run the group and sustain it for the next generation of students. Special thanks to Dilys Ruan for being my closest friend through all of this over the last three years. It has been a privilege to grow as people and as physicists together. Thanks to Anupam Mitra, Manuel Muñoz and Alex Mills for cheering us on and the many crazy lobby conversations. Finally, I would like to thank Dr. Seidel for supporting Dilys and I as we navigated the complicated world of REU and graduate school applications. You encouraged us to be confident as we took our first steps out into the professional world. After all of this, we beat the odds and are going to get our PhDs at Rutgers. Thanks to my family for encouraging me all throughout my time at UNM, and thank you UNM for giving me a home over the last four years in New Mexico.

Appendices

A Trajectory computation using Squad

This function performs spherical interpolation of a series of vectors of identical length. First, it prepares the quaternion representation of rotations that connect these vectors. Second, it provides the quaternions to the numpy-quaternion implementation of Squad and returns the keyframe vectors that represent the interpolated rotation. Written in Python 3.6.

```
import numpy as np
import quaternion # Requires the numpy-quaternion package

def SQUAD_unit_sphere(Vectors, n_timesteps):
    '''
    Vectors: The list of vectors defining points to interpolate
    rotations between
    n_timesteps: How many output timesteps would you like?

    This is currently broken for adjacent points that are angularly
    separated by more than  $\pi/4$ . The dot product check attempts to fix
    this but has been ineffective.
    '''
    # (axis 0, input vector index [0 -> # input vectors - 1]) (axis 1,
    element index [0 -> 2])

    # How many input vectors were supplied?
    n_int=np.shape(Vectors)[0]
    # Preparing the array that stores the angular separation between
    each vector and the initial vector
    angles=np.empty((n_int,1))
    # Preparing the array that stores the axis of rotation defined by
    the initial vector to each input vector
    axis=np.empty((n_int,3))
    # Preparing an array to store the quaternion representation of each
    rotation
    float_quat_array=np.empty((n_int,4))

    for i in range(n_int):
        if i==0: # First quaternion needs to represent no rotation
            angles[i]=0 # No rotation, zero angle
            axis[i,:]=np.array([0,0,0]) # No axis of rotation b.c. no
rotation
            float_quat_array[i,:]=np.transpose(np.array([1,0,0,0])) #
Identity quaternion, corresponds to no rotation
        else:
            # Compute the angular separation between the initial vector
            and the rest of the vectors
```

```

        angles[i]=np.arccos(np.dot(Vectors[0,:], Vectors[i,:])/(np.
linalg.norm(Vectors[0,:])*np.linalg.norm(Vectors[i,:])))
        # Compute the axis of rotation defined by the initial
vector and the rest of the vectors
        axis[i,:]=np.cross(Vectors[0,:], Vectors[i,:])/np.linalg.
norm(np.cross(Vectors[0,:], Vectors[i,:]))
        # Compute the quaternion representation of each rotation
        float_quat_array[i,:]=np.transpose(np.array([ np.cos(angles
[i]/2.), np.sin(angles[i]/2.)*axis[i,0], np.sin(angles[i]/2.)*axis[i
,1], np.sin(angles[i]/2.)*axis[i,2])))

        # Attempt to check for sign errors from large angular
separations
        dot=np.dot(Vectors[i-1,:], Vectors[i,:])
        if dot < 0.0:
            float_quat_array[i,:]=-float_quat_array[i,:]
            dot=-dot
            print('Bad_angle, _dot_product_is:', dot)

    # Convert float form of quaternion array to the proper quaternion
array format from numpy-quaternion
    quat_array=quaternion.as_quat_array(float_quat_array)

    # Assumes evenly spaced input times, could change this later on
    t_in = np.linspace(0.0,1.0,n_int)
    # Provides evenly spaced output times (i.e. when each keyframe is)
    t_out = np.linspace(0.0,1.0,n_timesteps)

    # Now that each quaternion has been prepared, feed into the
numpy-quaternion implementation of SQUAD to compute the quaternion
for each keyframe
    squad_out=quaternion.squad(quat_array, t_in, t_out)
    # Rotate the initial vector by all of the keyframe quaternions to
produce the vector at each keyframe. This creates the trajectory.
    vec_prime=quaternion.rotate_vectors(squad_out[:], Vectors[0,:])

    return vec_prime # Return the trajectory as a list of vectors.

```

B Animate angular dispersion, color by unitarity violation

This script animates the evolution of angular dispersion across x for increasing values of z , the radius. In addition, it also colors each point by the magnitude of unitarity violation at that point in the neutrino gas. The “LineModelAnalysis” package was a library I developed for loading and basic analysis of our two-angle and multi-angle line model simulations. In this script, LineModelAnalysis is only used to load the data and does not need to be described in detail. Written in Python 3.6.

```

from netCDF4 import Dataset
import numpy as np

```

```

import LineModelAnalysis
import matplotlib as mpl
mpl.use("Agg")
import matplotlib.pyplot as plt
from matplotlib.animation import FFMpegWriter

# Initialize my line model analysis library
lma=LineModelAnalysis.lma()

# Choose the ID of the dataset you want
choose=0

# Choose the angular bin (0 or 1 in two-angle line model)
use_rightgoing=0 # if 0, uses leftgoing

# Set the stride in Z, don't need every Z bin
z_Steps=100

# Select the dataset and load it into memory
lma.gen_dataset(choose, zSteps=z_Steps)
try:
    lma.initialize_dataset_in_memory(loadFresh=False, saveData=False,
    loadData=True)
except:
    lma.initialize_dataset_in_memory(loadFresh=True, saveData=True,
    loadData=False)

# Compute the magnitude of unitarity violation at each point in the
# neutrino gas
Unitarity_Violation_magnitude = np. abs(1-np.square(lma.mag_Pol_vector
[:,:,: , use_rightgoing]))

# Compute the angular dispersion between neighboring pol. vectors in x
Angular_Disp = .5*(
    np.arccos(np.divide(
        (np.multiply(np.roll(lma.P1[:,:,: , use_rightgoing], 1, axis=1), lma.
P1[:,:,: , use_rightgoing]))
        +(np.multiply(np.roll(lma.P2[:,:,: , use_rightgoing], 1, axis=1), lma.
P2[:,:,: , use_rightgoing]))
        +(np.multiply(np.roll(lma.P3[:,:,: , use_rightgoing], 1, axis=1), lma.
P3[:,:,: , use_rightgoing]))
        , np.multiply(np.roll(lma.mag_Pol_vector[:,:,: , use_rightgoing], 1,
axis=1), lma.mag_Pol_vector[:,:,: , use_rightgoing])))
    +
    np.arccos(np.divide(
        (np.multiply(np.roll(lma.P1[:,:,: , use_rightgoing], -1, axis=1), lma.
P1[:,:,: , use_rightgoing]))

```

```

        +(np.multiply(np.roll(lma.P2[:, :, use_rightgoing], -1, axis=1), lma
.P2[:, :, use_rightgoing]))
        +(np.multiply(np.roll(lma.P3[:, :, use_rightgoing], -1, axis=1), lma
.P3[:, :, use_rightgoing]))
        ,np.multiply(np.roll(lma.mag_Pol_vector[:, :, use_rightgoing], -1,
axis=1), lma.mag_Pol_vector[:, :, use_rightgoing]))
    )

# Preprate the animation writer
metadata = dict(title='Test', artist='Matplotlib',
                comment='Movie_support!')
writer = FFMpegWriter(fps=20, metadata=metadata)
fig = plt.figure()

# Stride in x to downsample by, keep at 1 please
downsample=1

# Define an empty plot object
plot_obj = plt.scatter([], [])

# Minimum unit. violation (log scale) to plot
min_y=6
plot_obj.set_clim(vmin=-min_y, vmax=np.max(np.log10(
    Unitarity_Violation__magnitude[:, :, downsample])))

# Set plot parameters, etc.
plt.xlabel('X_(km)', fontsize='small')
plt.ylabel('Angular_Dispersion_(radians)', fontsize='small')
plt.xlim((lma.xPos[0], lma.xPos[-1]))

plot_obj.set_cmap('magma')
k=0

# Plot ang. dispersion vs x, as the animation progresses along Z color
points by unit. violation
with writer.saving(fig, 'disp_color_by_unit_animation_min_'+str(min_y)+'
'+lma.name.strip('.nc')+'.mp4', dpi=360):
    i_final=int((lma.zFinal-lma.zStart)/z_Steps)
    for i in range(i_final):
        if np.max(np.log10(np.abs(Unitarity_Violation__magnitude[i, :]))
)>=-min_y:
            if k==0:
                print(np.nanmax(Angular_Disp[i:-1, :, downsample]))
                plt.ylim((0, np.nanmax(Angular_Disp[i:-1, :, downsample])))
            )

            i_start=i
            k=1

```

```

        plot_obj.set_offsets(np.transpose(np.array([lma.xPos[:, :
downsample], np.abs(Angular_Disp[i, : : downsample])]))))
        plot_obj.set_array(np.log10(Unitarity_Violation__magnitude [
i, : : downsample].ravel()))
        plot_obj.set_sizes([1]*len(lma.xPos[:, : downsample]))
        plt.title('Ang. Dispersion in X, colored by Unit. Violation
at Z='+str(np.around(lma.zPos[i], 2)), fontsize='small')
        if k==1:
            plt.colorbar(plot_obj)
            k=2
        writer.grab_frame()
        print(np.around(100*(i+1-i_start)/(i_final-i_start), 2))
writer.grab_frame()

```

References

- [1] Fermi, E. "Attempting a theory of beta rays." *I. Z. Physik* 88, 161-177 (1934): <https://doi.org/10.1007/BF01351864>
- [2] Cowan, C. L., Reines, F., Harrison, F. B., Kruse, H. W., McGuire, A. D. "Detection of the Free Neutrino: a Confirmation" *Science* Vol. 124. Num. 3212 (1956): pp 103-104.
- [3] Smirnov, A. Yu. "The MSW Effect and Matter Effects in Neutrino Oscillations." *Physica Scripta* T121 (2005): 57–64. Crossref. Web.
- [4] Faessler, A., Davis, R.. "Neutrinos in Cosmology, Astro, Particle and Nuclear Physics" .Elsevier Science (2016): pp 13-32.
- [5] Duan, H., Fuller G.M., and Qian, Y. "Collective Neutrino Oscillations." *Annual Review of Nuclear and Particle Science* 60.1 (2010): 569–594. Crossref. Web.
- [6] Duan, H. "Collective Neutrino Oscillations and Spontaneous Symmetry Breaking." *International Journal of Modern Physics E* 24.09 (2015): 1541008. Crossref. Web.
- [7] Duan, H. and Kneller, J. P. "Neutrino Flavour Transformation in Supernovae." *Journal of Physics G: Nuclear and Particle Physics* Vol. 36 Num. 11 (2009): 113201. Crossref. Web.
- [8] Duan, H., Fuller, G.M., and Qian, Y. "Simple Picture for Neutrino Flavor Transformation in Supernovae." *Physical Review D* 76.8 (2007): n. pag. Crossref. Web.
- [9] Duan, H., Fuller, G.M., and Qian, Y. "Collective Neutrino Flavor Transformation in Supernovae." *Physical Review D* 74.12 (2006): n. pag. Crossref. Web.
- [10] Duan, H et al. "Coherent Development of Neutrino Flavor in the Supernova Environment." *Physical Review Letters* 97.24 (2006): n. pag. Crossref. Web.
- [11] Duan, H and Fuller, G.M., and Carlson, J. and Qian, Y. "Analysis of collective neutrino flavor transformation in supernovae." *Phys. Rev. D* Vol. 75 Iss. 12 (2007): 125005. Crossref. Web.
- [12] Janka, H et al. "Theory of Core-Collapse Supernovae." *Physics Reports* 442.1-6 (2007): 38–74. Crossref. Web.
- [13] Meyer, B.S., McLaughlin, G., and Fuller, G.M. "Neutrino Capture And r-Process Nucleosynthesis." *Physical Review C* 58.6 (1998): 3696–3710. Crossref. Web.
- [14] Duan, H. et al. "The Influence of Collective Neutrino Oscillations on a Supernova r process." *Journal of Physics G: Nuclear and Particle Physics* 38.3 (2011): 035201. Crossref. Web.
- [15] Martin, J.D., Abbar, S., and Duan, H. "Nonlinear Flavor Development of a Two-Dimensional Neutrino Gas." *Physical Review D* 100.2 (2019): n. pag. Crossref. Web.
- [16] Shoemake, K.. "Animating rotation with quaternion curves." *SIGGRAPH Comput. Graph.* 19, 3 (1985), 245–254. DOI:<https://doi.org/10.1145/325165.325242>
- [17] Dam, E., Koch, M., and Lillholm, M. "Quaternions, interpolation and animation". Tech. rep. DIKU-TR-98/5 (1998) University of Copenhagen.

- [18] Duan, H., and Shalgar, S.. “Flavor Instabilities in the Neutrino Line Model.” *Physics Letters B* 747 (2015): 139–143. Crossref. Web.
- [19] Abbar, S., Duan, H., and Shalgar, S.. “Flavor Instabilities in the Multiangle Neutrino Line Model.” *Physical Review D* 92.6 (2015): n. pag. Crossref. Web.